energies

MDPI

Article

Fuzzy-Logic-Controlled Hybrid Active Filter for Matrix Converter Input Current Harmonics

Asare Koduah [1,*] and Francis Boafo Effah [2]

[1] Department of Electrical Power System, Kaunas University of Technology, 51394 Kaunas, Lithuania
[2] Department of Electrical Engineering, Kwame Nkrumah University of Science and Technology, Kumasi 00233, Ghana
* Correspondence: asakod@ktu.lt

Abstract: The proliferation of matrix converter interfaces coupled with traditional loads produces nonstandard and high-frequency harmonics in the range of (2 to 150) kHz in the power system. Although several research works have been conducted on passive and active filter solutions, most of these are low-frequency (below 2 kHz) solutions and are not effective under supraharmonic frequencies. An experimental study of a fuzzy-inference-system-controlled hybrid active power filter (HAPF) for the attenuation of higher frequency harmonics (above 8 kHz) is proposed. The compensational approach introduced is different from traditional approaches and the use of the fuzzy logic controller eliminates complexities involved in active filter designs. The proposed filter obtained a total harmonic distortion (THD) of 1.16% of the fundamental 50 Hz supply frequency. The performance of the proposed hybrid filter was compared with that of the proportional and integral (PI) controlled topology. The results obtained indicated superior performance of the fuzzy logic controller over the PI in terms of compensational speed, accuracy, the THD of the supply current and the overall integrity of the matrix converter. Illustrative design blocks and simulation in MATLAB/Simulink environment are provided to buttress these findings.

Keywords: active harmonic filter; hybrid harmonic filter; matrix converter; passive filter

Citation: Koduah, A.; Effah, F.B. Fuzzy-Logic-Controlled Hybrid Active Filter for Matrix Converter Input Current Harmonics. *Energies* **2022**, *15*, 7640. https://doi.org/10.3390/en15207640

Academic Editor: Gabriel Nicolae Popa

Received: 25 September 2022
Accepted: 14 October 2022
Published: 16 October 2022

1. Introduction

Since their introduction in the 1970s, matrix converters (MC) have gained popularity due to their many applications [1]. However, they produce significantly higher frequency harmonic pollution, around their switching frequency, in the supply. These high frequencies are due to their large number of switching states and switching frequency. The switches of the MC are required to block voltages and conduct currents bidirectionally. This is because the MC is mostly fed by a voltage source, hence its input terminals must not be short circuited. Connected loads, to the MC, are mostly inductive in nature, and hence the output terminals must also not be open circuited. With the above conditions, the total switching states required to implement the MC are reduced from 512 to 27. Irrespective of this, its protection scheme is that of a simple, relatively lower cost hardware architecture. Several research works have been conducted on the MC due to its wide application [1,2], particularly in applications where weight and size are of much concern such as in electric vehicles, aircraft, ships and submarines. Other research works are focused on improving its voltage transfer ratio of 0.867, regarding which several research works have successfully obtained more than unity voltage transfer ratio [3–7].

In a typical power system, domestic and industrial nonlinear loads result in harmonic pollution of the source voltage and current. The presence of these harmonic voltages and currents in the power system may result in copper, iron and dielectric losses. Transformers and rotating machines may experience heating, dielectric stress, hysteresis and eddy current losses due to the presence of voltage harmonics [8]. Capacitor banks may experience

overloads. Protective relays' time delay characteristics are deteriorated in the presence of harmonics [9]. Although higher frequency switching of power converters results in relatively smaller sizes for design components, they tend to produce higher switching losses and frequency harmonics for which passive filters may not be adequate to minimize [10]. Relatively higher frequency harmonics from cycloconverters are also challenging to compensate by the shunt active power filters (SAPF) due to non-availability of required switches and economic considerations [6,11]. The presence of these higher frequency harmonics poses threats to the nonlinear loads themselves, as well as to sensitive electrical loads such as industrial controllers, hospital equipment and laboratory and experimental setups [12–14]. Also, high losses may be recorded in utility transformers, transmission lines and motors. Relay settings are also susceptible to high frequency ac line harmonics.

The objectives and contributions of this paper are:

1. To propose a HAPF consisting of a SAPF and a series passive R-L-C filter.
2. To obtain a THD within the recommended IEEE 519-2014 requirements with faster dynamic response time using fuzzy inferencing system.
3. Separation of the high frequency currents was accomplished in the $\alpha - \beta$ domain using a second order analogue filter with cutoff frequency of 30 Hz.

The remainder of this paper is arranged as follows: Section 2 is a review of selected literature on the topic. The methodology used is introduced and explained in Section 3, which involves four subsections. Section 3.1 explains the mathematical modelling and analysis of the passive section of the proposed HAPF, while Section 3.2 introduces the design of the active section. Sections 3.3 and 3.4 address the reference current extraction and the control strategies used in the design. Section 4 summarizes the experimental simulations and obtained results while Section 5 discusses the obtained results. Section 6 concludes the study with future research directions.

2. Review of Selected Literature

Periodic voltages and currents with frequencies that are integer multiples of the fundamental supply frequency are termed as harmonic voltage or current, respectively. Supply voltage harmonics are mostly a result of supply impedance and load current distortions [15]. The supply current harmonics are mostly due to the nonlinearity of connected load, as experienced in AC/DC converters and controls of industrial and domestic appliances. Cell phone chargers, laptop chargers and all DC loads which require rectifier circuits and power semiconductor switches are the primary sources of harmonic currents in the power system [16,17]. Due to the fact that DC supply is not readily available, various international bodies have proposed standards for minimum harmonic production of various manufactured electric and electronic products. The IEEE-519-1992 recommends a maximum 5% harmonic content for voltages below 65 kV [18]. The European harmonic standard, IEC-555, also recommends an absolute harmonic limit for all consumer manufactured loads [8].

The harmonic disposition of the voltage and current and their characteristics can be identified at the point of common coupling (PCC) and corrective measures implemented. Traditionally, passive filters were used in mitigating power quality issues, specifically, harmonics [6]. The authors of [19] performed a numerical investigation on the stability of an electric drive system coupled with a passive LC filter topology with a dumping resistor parallel to the inductor, to form an RLC filter topology. The RLC filter was put in series with a MC feeding a three-phase symmetrical R-L load. They concluded that their proposed model maintained the stability of the MC during harmonic compensation. However, because the damping resistance was limited to a minimum value of 4 Ω, there was a significant reduction of the output power limit of the MC. Also, the authors of [20] supplemented the traditional passive RLC filter with a relatively small capacitor in series to the damping resistor in the RLC topology to form a CLCR filter. The authors concluded that the frequency response characteristics of the CLCR topology were relatively lower compared with the traditional RLC topology. Hence, their topology had a harmonic damping rate with a decrease of THD level of 13–16%. Although the increase of the overall

capacitance may result in further deterioration of the input power factor, these were skipped and very little was said about it by the authors.

Furthermore, in [21,22] the authors presented Lyapunov-controlled-matrix-based unified power flow controllers coupled at the input side with a passive RLC filter. Their model improved the steady state errors. Their obtained THD for the line current and voltage were 4.86% and 4.53% of the fundamental frequency, respectively. However, the disadvantages of passive filters are well known and have been explored extensively by [23], and they range from their bulky size and non-reliability to the risk of resonance with the line impedance. Their fixed compensational property diminishes their advantages in an ever growing and dynamic load system. The problem of consistent component (capacitor) replacement with load changes also affects their use. To overcome these challenges, active power filters (APF) have been proposed by researchers.

The authors of [1,24] modelled an SAPF for supply current harmonic reduction in matrix converters. They employed the instantaneous reactive power control theory for the generation of compensation currents. Although the authors did not specifically state the numerical THD of their obtained results, analysis of their input current waveform suggests a THD of not less than 25% of their fundamental frequency. The authors did no analysis on the effects of their filter on the voltage transfer ratio or on the dynamic performance of the MC.

The authors of [2,7] focused on HAPF and heuristic approaches in harmonic mitigations in order to harness the advantages of both active and passive filters. Ref. [2] presented a topology without the use of input or output filters, rather being based on the modulation of the matrix converter by feedforward and fuzzy logic control (FLC) system feedback method. In their model, the input and output voltage and current parameters of the MC were measured and compared with referent values to modulate the matrix converter appropriately. Although this model worked correctly to maintain the voltage transfer ratio of the MC and reduce harmonics, the stability and output power limit are questionable. Also, the response time of the MC needs to be investigated as well as the overall power factor since there was no analysis done to verify the effects on these parameters.

On the other hand, Ref. [7] modelled a HAPF comprising two active power filters separately controlled (shunt and series active filters). The SAPF was modelled for the input side harmonics to compensate the supply current ripples and the series active filter for the output voltage ripples of the MC. The authors concluded that there were 18% input current harmonic distortions and 3% output voltage distortions of their fundamental 60 Hz supply frequency. The problem with their model was the use of two active filters with separate control strategies which are likely to generate undesired higher frequency components at their switching frequencies and tend to slow down the response of the coupled converter.

The authors of [25] proposed an advance common control method for a HAPF topology consisting of two active filters (shunt and series filters) for a six-pulse thyristor rectifier. The authors recommended an improved reference signal tracking (RST) control architecture to overcome phase lag effects often associated with this type of hybrid filter topologies. In all, their work showed promising results with 1.5% THD and it was within the accepted 5% recommendations per IEEE values. Irrespective of this, their solution may not be applicable to the MC. Table 1 shows similar works on the harmonic mitigations by some authors and their results.

Table 1. Summary of reviewed literature.

References	Filter Type	Topology	THD%	Limitations
[1,14]	Active	Shunt active	>20	Reduced power limit
[19]	Passive	R-L-C	<15	Reduced power limit at Rd < 4 Ω
[20]	Passive	CLCR	<16	Poor power factor, power limited below Rd < 4 Ω
[21,22]	Passive	R-L-C	<16	Reduced power limit at Rd < 4 Ω
[2]	Hybrid	FIS	4.16	Not stable

Table 1. *Cont.*

References	Filter Type	Topology	THD%	Limitations
[7]	Hybrid	Shunt and series active filters	18 and 3	Slow response
[25]	Hybrid	Shunt and series active filters	1.5	Good performance

3. Methodology

This research considers a 400 $V_{L\text{-}L}$ 50 Hz, three-phase balanced supply connected to a resistive load through a MC with power rating (S_{MC}) and switching frequency of 50 kW and 8 kHz, respectively. The input to the MC is connected to the passive filter section of the hybrid filter. This is to reduce the infinite rate of change of the MC input current to a finite rate of change to enable the SAPF to compensate the harmonics effectively. Figure 1 shows the proposed HAPF. The components of the supply current, due to the converter, are the DC component, active and reactive powers, as well as harmonics, as illustrated in (1).

$$i_S(t) = i_L(t) = i_0 + i_1 \sin(\omega t + \theta_1) + \sum_{n=5,7.9.11...}^{\infty} i_n \sin(n\omega t + \theta_n) \quad (1)$$

where

$i_{S(t)}$: Supply current.
$i_{L(t)}$: Load current.
i_0: DC current component.
i_1: First harmonic component.
ω: Angular frequency.
θ: Phase shift.
n: Harmonic number.

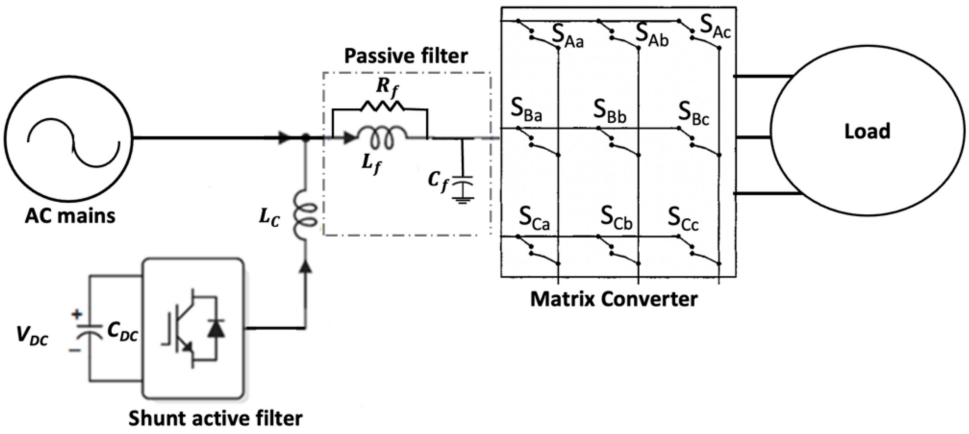

Figure 1. Proposed HAPF architecture.

3.1. Design of Passive LC Filter Section of the HAPF

For an effective implementation of the HAPF, the passive filter must be designed to reduce the rate of change of the input current and attenuate the higher order harmonics while the active filter compensates the lower order harmonics, particularly the 5th, 7th, 11th and 13th harmonic range [26]. The design therefore consists of the two sections: the passive filter section and the SAPF section. A power system consisting of an LC filter in series with the MC and a resistive load was considered. Figure 2 shows the series connection of the passive LC filter and its equivalent circuit diagram.

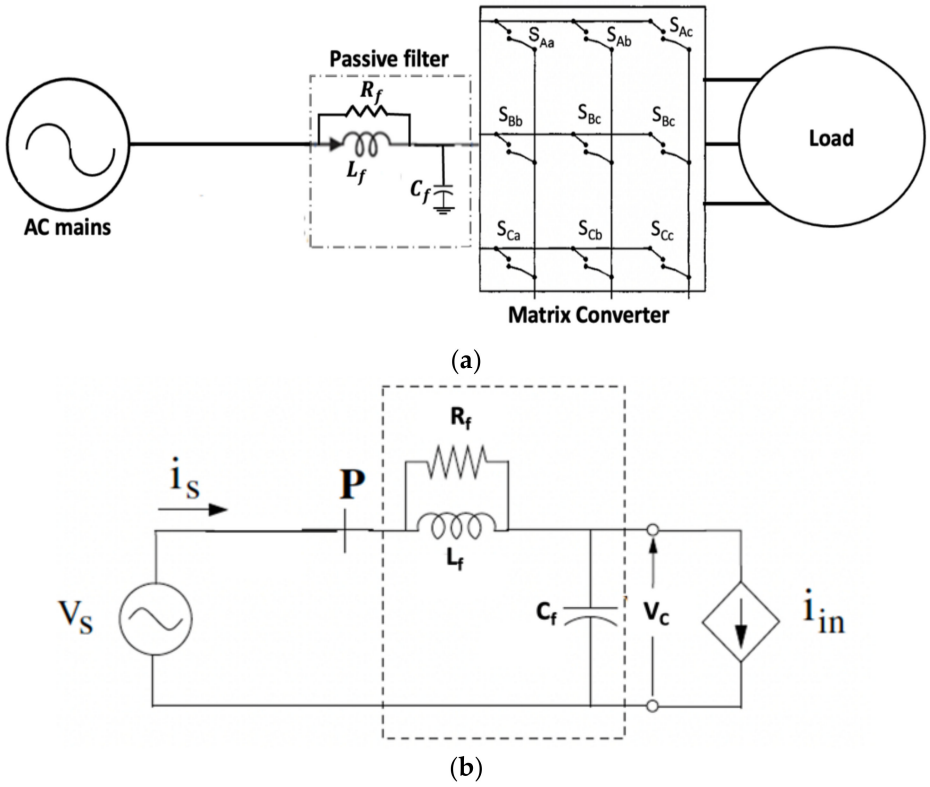

Figure 2. Passive LC filter for MC input harmonic mitigation: (**a**) single line diagram; (**b**) equivalent circuit diagram.

From Figure 2b, the transfer function of the passive filter can be represented under the following equation sequence:

$$G(j\omega) = \frac{j\omega\frac{L_f}{R_f} + 1}{1 - \omega^2 L_f C_f + j\omega\frac{L_f}{R_f}} \tag{2}$$

$$|G(j\omega)| = \sqrt{\frac{1 + \frac{r_\omega^2}{Q^2}}{\left(1 - r_\omega^2\right)^2 + \frac{r_\omega^2}{Q^2}}} \tag{3}$$

where

$$r_\omega = \frac{\omega}{\omega_C} \quad Q = R\sqrt{\frac{C_f}{L_f}} \tag{4}$$

with

V_S: Supply voltage.
i_S: Supply current.
P: Point of common coupling.
L_f: Filter inductance.
C_f: Filter capacitance.
R_f: Damping resistor.

The filter values were selected with respect to established constraints of the maximum attenuation of the filter to be less than 26 dB. Again, the criteria for selecting the filter inductance was based on 5% voltage drop over the filter inductance, and 10% of I_{MC} represents the reactive currents over the filter capacitor. A damping resistor of 0.5 Ω was

selected. These constraints will restrict the high rate of change (di/dt) of the MC input current. The filter elements C_F and L_F, as well as the MC input current, were calculated as:

$$I_{MC} = \frac{S_{MC}}{\sqrt{3}V_S} = \frac{50e3}{400\sqrt{3}} = 72 \text{ A} \quad (5)$$

$$C_f \leq \frac{0.866K_C I_{MC}}{\omega_g V_S} = \frac{0.1 \times 72 \times 0.866}{2pi \times 50 \times 400} = 49.6 \text{ µF} \quad (6)$$

$$L_f \leq \frac{K_L V_S}{\omega_g \sqrt{(i_{in}^2 + i_c^2)}} = \frac{0.05 \times 400}{2\pi \times 50 \times \sqrt{(i_{in}^2 + i_c^2)}} = 1 \text{ mH} \quad (7)$$

3.2. Design of Active Section of HAPF

The design of the active section of the HAPF includes the power stage and the control strategy. The power stage consists of an IGBT with anti-parallel diodes voltage source converter (VSC). Current source converters (CSC) could be used but would require extra design modifications as IGBTs with series diodes are not readily available. The design of the VSC consists of three component selections:

1. The selection of the DC voltage, V_{dc}.
2. The selection of coupling inductance, L_c.
3. The selection of the DC side capacitance, C_{DC}.

3.2.1. Selection of V_{dc} and L_c

The selection of V_{dc} and L_c required the assumption that the supply ac voltage remained sinusoidal under all conditions. Also, the peak-to-peak ripple line current distortions were assumed to be 5% of the capacitor current. Finally, the PWM inverter was assumed to operate in the linear modulation mode.

From Figure 3, it can be seen that the HAPF must adjust the inverter current, i_{inv}, to compensate the reactive power in (1). An efficient compensation will result in the supply current, i_s, being in phase with the supply voltage, V_s, and the inverter current, i_{inv}, being orthogonal to the supply voltage, as seen in Figure 3b.

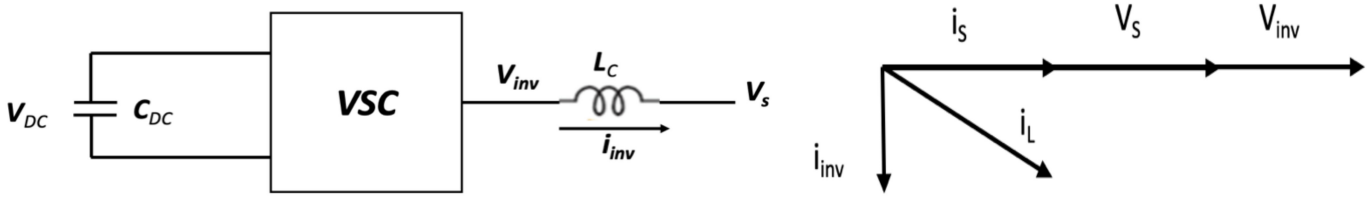

(**a**) (**b**)

Figure 3. Active power filter (HAPF) architecture: (**a**) reactive power flow; (**b**) vector diagram.

Again, from Figure 3, the reactive power produced by the inverter can compensate the reactive power in the supply when $V_{inv} > V_s$ under linear modulation mode [27]. The capacitance voltage, V_{dc}, was obtained as:

$$m_a = \frac{2\sqrt{2}V_{inv}}{V_{dc}} \quad (8)$$

If $m_a = 1$, then:

$$V_{dc} = 2\sqrt{2}V_{inv} = 2\left(\sqrt{2}/\sqrt{3}\right)Vs = 653 \text{ V} \approx 700 \text{ V} \quad (9)$$

The coupling inductance, L_c, filters out the ripples in the inverter output current and limits the high rate of change of the inverter current. Hence, its selection was based

on the peak-to-peak ripple current, i_{ripp}, which was calculated as (10). From Figure 4, and considering the period of the current change as 10% of the MC switching period (1/8 kHz = 1.25×10^{-4}), the harmonic currents are assumed to be 10% of the input current to the MC, and then the maximum di/dt of the inverter current can be calculated as:

$$max\left|\frac{di_L}{dt}\right| = \frac{72 \times 0.1}{1.25 \times 10^{-4}} = 0.576 \times 10^6 \text{ s} \quad (10)$$

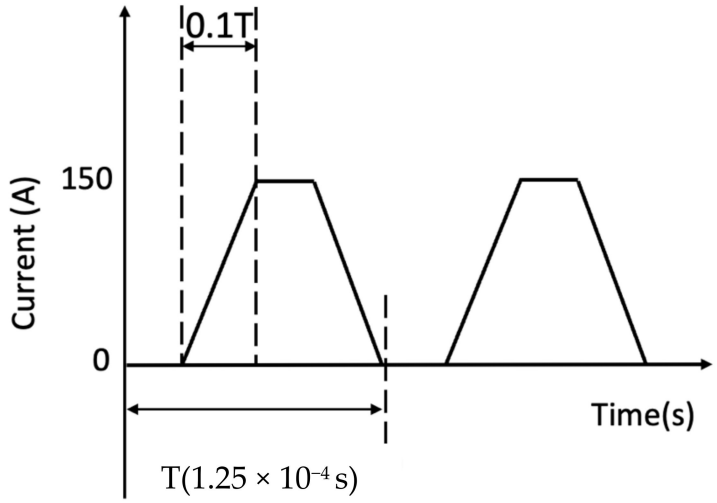

Figure 4. Theoretical input current rate of change after passive filter.

Hence, from (11), minimum *Lc* can be obtained as:

$$L_C \geq \frac{\frac{2}{3}V_{dc} - V_s}{max\left|\frac{di_L}{dt}\right|} = 115 \text{ µH} \quad (11)$$

3.2.2. Selection of the DC Capacitance

The selection of the DC capacitance value was based on the instantaneous power exchange between the inverter and the grid during transients. The peak-to-peak ripple voltage of the inverter was assumed to be 15% of the DC bus voltage. Hence, the lost energy in the inverter is compensated for as:

$$E = \frac{1}{2}C_{dc}\left(V_1^2 - V_2^2\right) \quad (12)$$

where $V_2 = V_1 - \Delta V_{ripp}$ and ΔV_{ripp} is the peak-to-peak ripple voltage. V_1 is the DC voltage. If the power rating of the inverter is P, then the energy stored in the capacitor for a period T can be estimated by:

$$E = P \times T \quad (13)$$

$$\frac{1}{2}C_{dc}\left(V_1^2 - V_2^2\right) = P \times T = K3V_S I_f aT = 5624.9 \text{ µF} \quad (14)$$

where

a: Overload factor (1.2).
Vs: Phase voltage.
I_f: Active filter ac side current.
T: Recovery period (30 ms).
K: Proportionality constant (0.1).

3.3. Control and Reference Current Extraction for the SAPF

The effectiveness of the SAPF is dependent on the appropriate control strategy used for the generation of compensational currents as well as gating signals for the voltage source inverter. Voltage and line current measurements were obtained to extract the reference currents. The instantaneous reactive power (P-Q) theory proposed by [28] was used to generate the compensating currents in the time domain. Finally, the gating signals for the voltage source inverter were generated using the hysteresis current loop control.

The instantaneous reactive power theory gives the flexibility of deciding the kind of compensation required. There are basically two kinds:

1. Total compensation.
2. Partial compensation.

Total compensation involves reactive power compensation, harmonic attenuation, power factor correction and three-phase power system balancing. Total compensation is mostly recommended for low power applications (Akagi, 2005). Implementing reactive power compensations in high power applications is not an economically viable option due to the current and voltage magnitudes that will be handled.

Partial compensation is mostly recommended for harmonic content compensation only. It includes either the voltage, current or both harmonic contents compensation. Most publications are about partial compensation since it is implemented in low power applications. The shape of the supply voltage is crucial in both the current and voltage harmonic compensations. A distorted supply voltage waveform increases the cost and difficulty in current harmonic compensations. In most cases, phase locked loop (PLL) circuits are recommended for unbalanced and distorted supply voltage applications. From (1), the magnitude of the instantaneous complex power (S) can be given as:

$$s = p + jq = 3/2v(t)i^*(t) \tag{15}$$

where

s: Instantaneous complex power.
$v(t)$: Instantaneous voltage vector.
$i(t)$: Instantaneous current vector.
p: Active power.
q: Reactive power.

With the instantaneous space vectors of the voltage and current represented as 'v' and 'i', respectively, then the current space vector can be expressed as

$$i(t) = {}^2/_3\frac{v}{|v|^2}S^* = {}^2/_3\frac{v}{|v|^2}(p - jq) \tag{16}$$

with

$$|v|^2 = v_\alpha^2 + v_\beta^2 \quad \text{in the } \alpha - \beta \text{ domain}$$

The active and reactive powers (p and q) can be decomposed into their direct and oscillatory components, where;

$$P = \widetilde{P} + \overline{P} \quad and \quad Q = \widetilde{q} + \overline{q} \tag{17}$$

with

S*: Desired apparent power.
$\overline{P}$ and $\overline{q}$: Direct component of the active and reactive power.
$\widetilde{P}$ and $\widetilde{q}$: Oscillatory component of the active and reactive power.

Equation (16) was used to calculate the reference current in the SAPF topology. By the instantaneous reactive power theory, the desired apparent power vector has two com-

ponents: the direct component and the oscillatory component for both the instantaneous active and reactive powers as seen in (18):

$$S_{desired} = \begin{cases} \widetilde{p} - j\widetilde{q} & Partial\ compensation \\ \widetilde{p} - jQ & Total\ compensation \end{cases} \tag{18}$$

From (18), the compensation of the oscillatory components of the instantaneous active and reactive powers of the desired complex power will result in partial compensation, while the compensation of the oscillatory component of the instantaneous active power and the instantaneous reactive power will result in total compensation by the SAPF. This research was based on total compensation of the desired apparent power.

The instantaneous P-Q theory involves the transformation, using the Clarke and its inverse transformations, of the three-phase a-b-c reference frame into a two-phase orthogonal stationary reference frame, α-β-0, as referred to in (19)–(21). Figure 5 depicts the transformation.

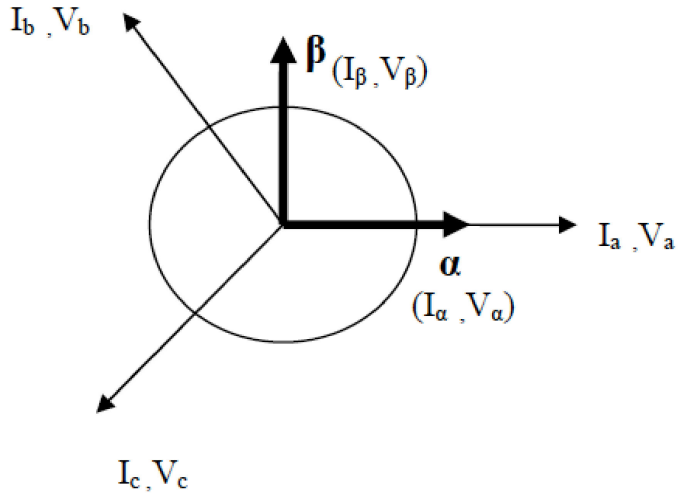

Figure 5. Three-phase a-b-c to $\alpha - \beta$ transformation.

$$\begin{bmatrix} i_\alpha \\ i_\beta \\ i_0 \end{bmatrix} = \sqrt{\frac{2}{3}} \begin{bmatrix} 1 & -1/2 & -1/2 \\ 0 & \sqrt{3}/2 & -\sqrt{3}/2 \\ 1/2 & 1/2 & 1/2 \end{bmatrix} \begin{bmatrix} i_{La} \\ i_{Lb} \\ i_{Lc} \end{bmatrix} \tag{19}$$

$$\begin{bmatrix} i_{Ca} \\ i_{Cb} \\ i_{Cc} \end{bmatrix} = \sqrt{\frac{2}{3}} \begin{bmatrix} 1 & 0 & 1/\sqrt{2} \\ -1/2 & \sqrt{3}/2 & 1/\sqrt{2} \\ -1/2 & -\sqrt{3}/2 & 1/\sqrt{2} \end{bmatrix} \begin{bmatrix} i_\alpha \\ i_\beta \\ i_0 \end{bmatrix} \tag{20}$$

and

$$\begin{bmatrix} p \\ q \end{bmatrix} = \begin{bmatrix} V_\alpha & V_\beta \\ V_\beta & V_\alpha \end{bmatrix} \begin{bmatrix} I_\alpha \\ I_\beta \end{bmatrix} \tag{21}$$

The harmonic contents of the apparent power were extracted using low pass filters [29]. Reference currents were then derived from the extracted harmonic contents by means of the inverse Clarke transformation. The inverter gating signals were generated by comparing the reference currents with the inverter currents by means of the hysteresis current loop, as shown in Figure 6. The reference current falls within the hysteresis band (HB), bounded above and below by setpoints.

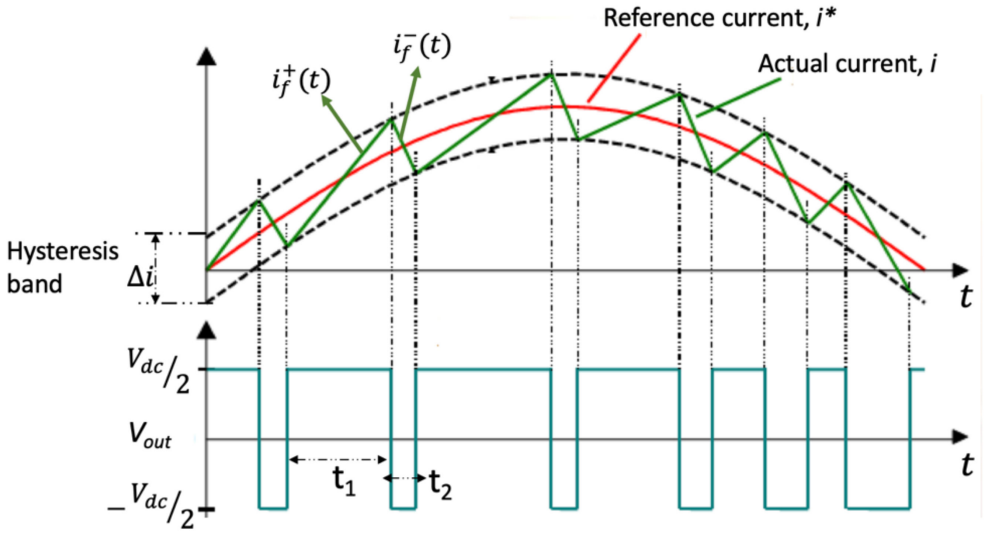

Figure 6. Hysteresis current loop control.

The generated compensating currents are 180° out of phase with the load current and contain the harmonics required by the load currents. Hence, the supply current is rendered free from the load harmonics, as depicted theoretically in (23).

$$i_S + i_{SH} = i_L + i_{LH} - i_C \tag{22}$$

with

$$i_S = i_L + i_{LH} - (i_{LH} - i_{SH}) - i_{SH} \tag{23}$$

where

i_{SH}: Supply current harmonics.
i_{LH}: Load current harmonics.
i_C: Compensational current.

3.4. Fuzzy Inferencing Control System (FIS)

One of the most important factors for classification of active harmonic filters is the regulation of the DC capacitor voltage. There is the need to maintain constant capacitor voltage so as to control the dynamic performance as well as the overall performance of the active filter. Traditionally, PI controllers are used for this function. The complexity in linearizing the system to tune the PI controller and its integral delay diminishes the usefulness of the PI controller as the control algorithm for the DC capacitor voltage. This research employed the FIS control model to regulate the DC capacitor voltage and compared its performance with that of the PI-controlled version. The selection of FIS over PI controllers was based on the avoidance of the complex tuning processes associated with PI controllers. Also, the simplicity and faster response time during transients, as well as better voltage tracking, encouraged the use of FIS controllers over the PI controller architecture.

Fuzzy logic enables computers to mimic human reasoning in quantifying incomplete and imprecise data to achieve definite conclusions. The authors of [30] presented extensive work on the implementation and architecture of fuzzy logic controls and further explanation of the topic can be obtained in their work. Figure 7a summarizes the FIS in a synoptic diagram, and Figure 7b shows its architecture for controlling the DC capacitor voltage in the proposed HAPF using MATLAB/Simulink building blocks.

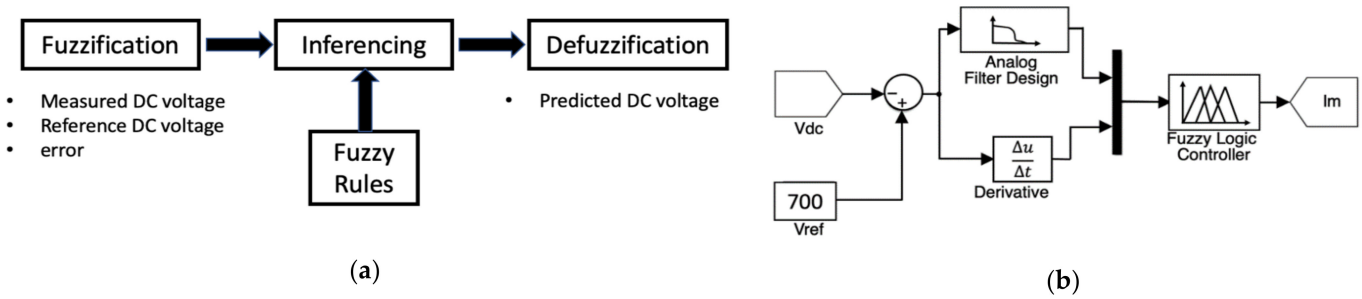

Figure 7. (**a**) Synoptic fuzzy inference architecture; (**b**) DC capacitor voltage control block.

The DC capacitance voltage, V_{dc}, is compared with its reference, V_{ref}, and the error, e_{rr} ($V_{ref} - V_{dc}$), and its rate of change were used as the inputs to the fuzzy controller. The output of the fuzzy controller is added to the active power compensation block in the instantaneous power calculation. This increases the active power drawn from the supply just enough to compensate for the losses in the inverter operation.

The fuzzification process converted the input and output variables, in this case the DC capacitor voltage error and its rate of change, into linguistic fuzzy sets. These sets are assigned membership values based on the Mamdani style of referencing which indicates the level of belongingness. Figure 8a shows the adopted triangular membership functions and seven sets or levels of belongingness: more negative (MN), negative (N), partially negative (PN), zero error (Z), partially positive (PP), positive (P) and more positive (MP). Figure 8b shows the output of the fuzzy process in a surface plot view. The inferencing process involves a set of rules to control the FIS input to output coordination through modus ponens means. Table 2 shows the rules generated for the implementation. The degree of truth that a particular input has with the rules is measured and contributes to a specific output behavior [27,31,32]. The output of the FIS is finally converted into crisp values to be interpreted. The process of converting the FIS output into crisp quantities is the so-called defuzzification process.

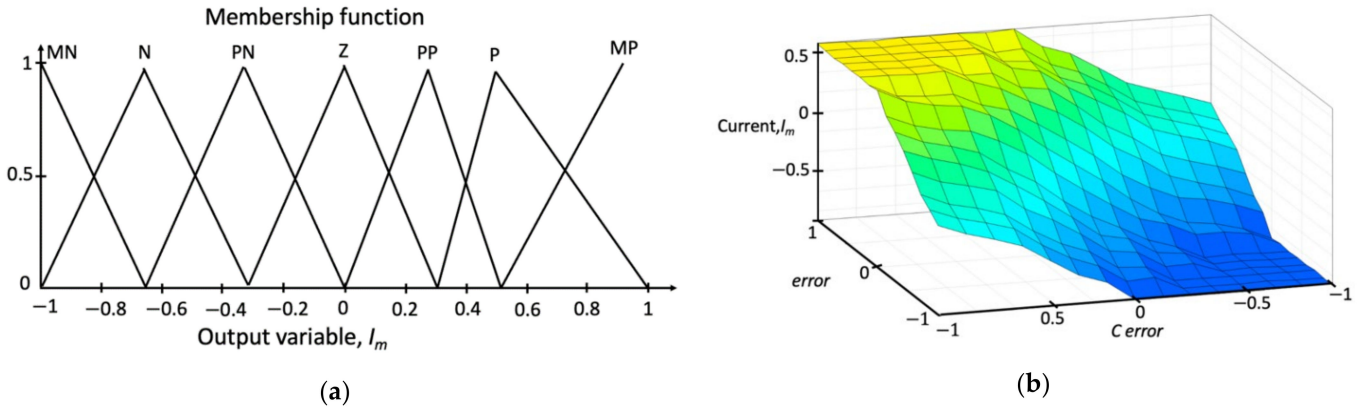

Figure 8. (**a**) Level of membership function; (**b**) filter output as shown in surface view.

Table 2. FIS rule table.

	MN	**N**	**PN**	**Z**	**PP**	**P**	**MP**
MN	MN	MN	MN	MN	N	PN	Z
N	MN	MN	MN	N	PN	Z	PP
PN	MN	MN	N	PN	Z	PP	P
Z	MN	N	PN	Z	PP	P	MP
PP	N	PN	Z	PP	P	MP	MP
P	PN	Z	PP	P	MP	MP	MP
MP	Z	PP	P	MP	MP	MP	MP

4. Simulation and Results

The proposed HAPF was modelled in MATLAB/Simulink environment as shown in Figure 9. It consists of the parallel combination of a SAPF and an RLC filter in series to the input side of the MC. The model was simulated for 150 ms. The SAPF is only activated after 20 ms of simulation time by means of a circuit breaker action. Table 3 shows the parameters for the simulation.

Table 3. Simulation parameters.

Parameter	Value
Supply voltage ($V_{L\text{-}L}$)	400 V, 50 Hz
Matrix converter	50 kW, 8 kHz
LC low pass filter values, L_F, C_F	1 mH, 50 μF
DC reference voltage, V_{dc}	677.69 V min, 700 V max
Coupling inductance, L_{inv}	115 μH
DC capacitance, C_{DC}	600 μF

Equations (18)–(21) were used to separate the higher frequency current harmonics from the load current to generate reference currents. These generated reference currents are opposite and 180° out of phase with the load current. Hence, the algebraic sum of the load current and the reference current signals result in the fundamental supply current. This proves the effectiveness of the alpha–beta transformation. Figure 10 illustrates the simulated results obtained under the principle in MATLAB/Simulink, with the compensation current, load current and the sum as I_C, I_L and their sum, respectively.

An R-L load of similar rating was coupled to the load by means of a three-phase breaker which activated after 50 ms. It was observed that the proposed HAPF topology obtained harmonic compensation within half a cycle of the activation of breaker 2. All results obtained showed no phase lag between the voltage and the supply current. However, with the introduction of distorted supply voltages, a minimal lag was observed. This was corrected with the introduction of a phase locked loop (PLL) in the control design. The passive input filter impedance was carefully designed to attenuate the high-frequency harmonics enough to maintain the stability of the MC by reducing the passive filter capacitance.

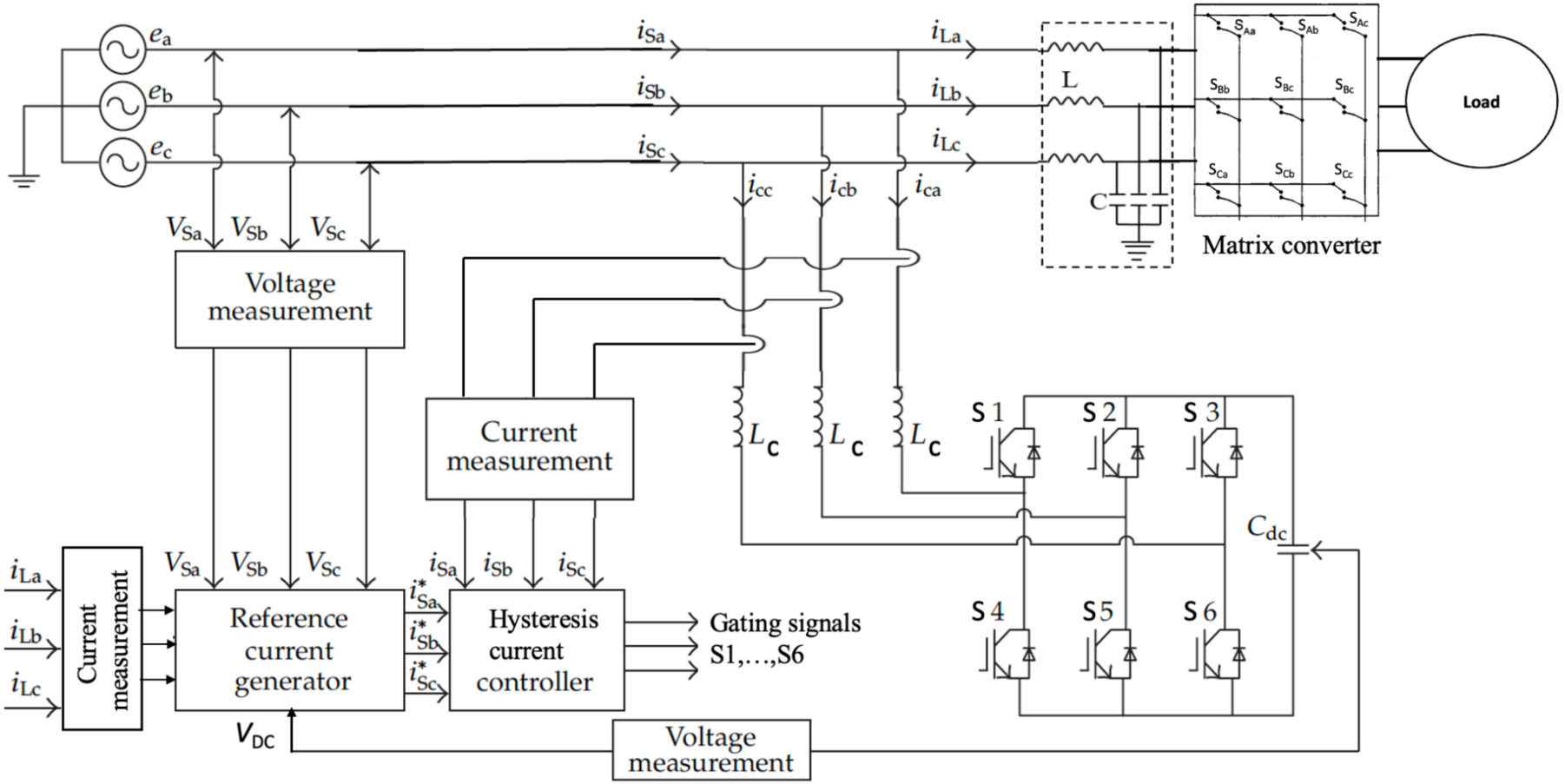

Figure 9. FIS-controlled HAPF architecture in MATLAB/Simulink environment.

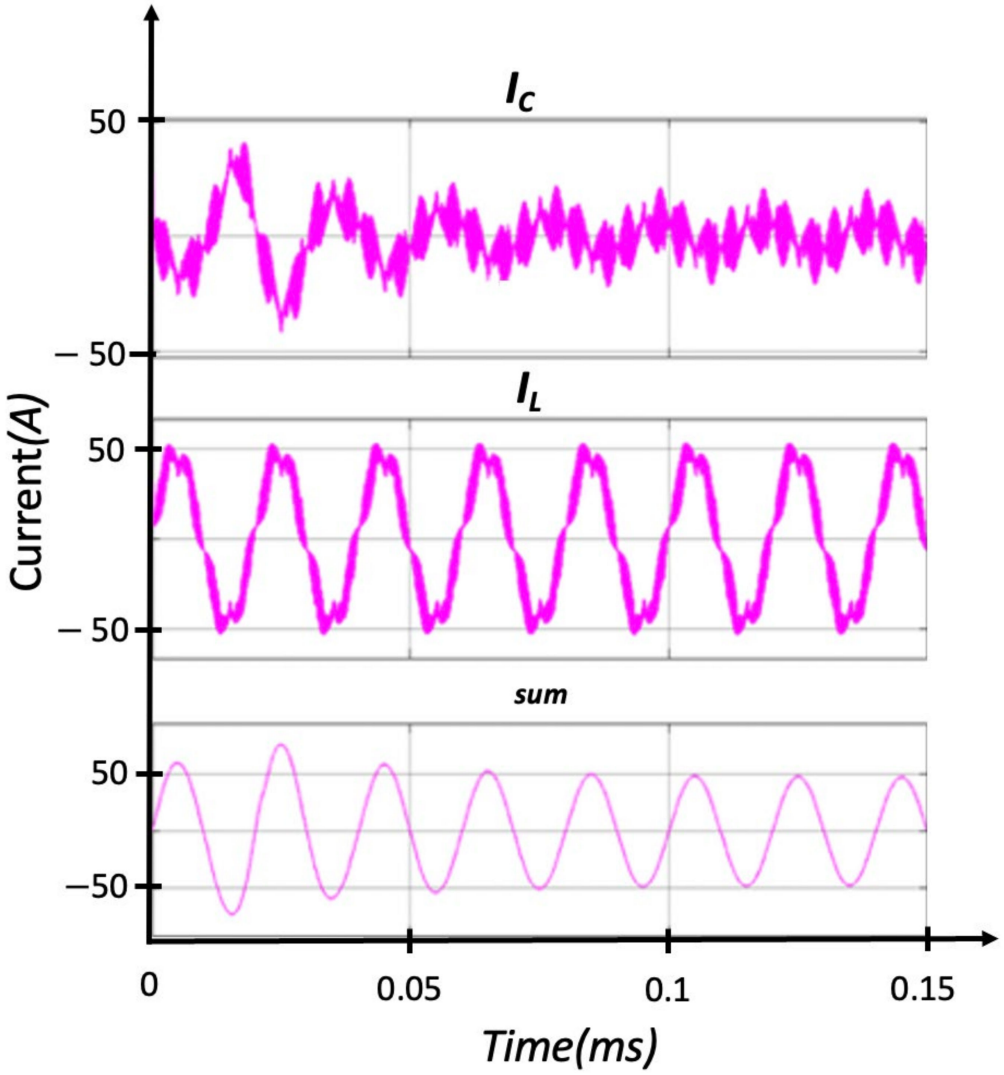

Figure 10. High-frequency error separation.

5. Discussion

Figure 11a shows the three-phase supply voltage (V_S) and current (I_S), as well as the load current (I_L) of the setup without any filter. It can be observed that the supply current is rich in high-frequency harmonics. These harmonics are obviously from the load current. FFT analysis of the supply current as well as the load current shows a 56.88% THD. High-frequency harmonics of a magnitude of 19.56% of the fundamental were observed at the switching frequency of the MC, as can be seen from Figure 12a. The simulation was performed with three different switching frequencies of the MC (6, 8 and 10) kHz. In all control experiments, the high frequencies were observed around the switching frequency of the MC. It was then concluded that the high frequencies propagated from the MC. Figure 11b shows the setup with the passive filter only. It was observed that the passive RLC filter successfully attenuated the high frequencies from 56.88% to 17.29% THD, and the higher frequencies from 19.56% to 7.64% THD, as could be observed from Figure 12b. The passive filter could not have further filtered without affecting the input power quality and the maximum power transfer of the MC. With these values as the new set point, the active filter now has a much lower rate of change of the input current.

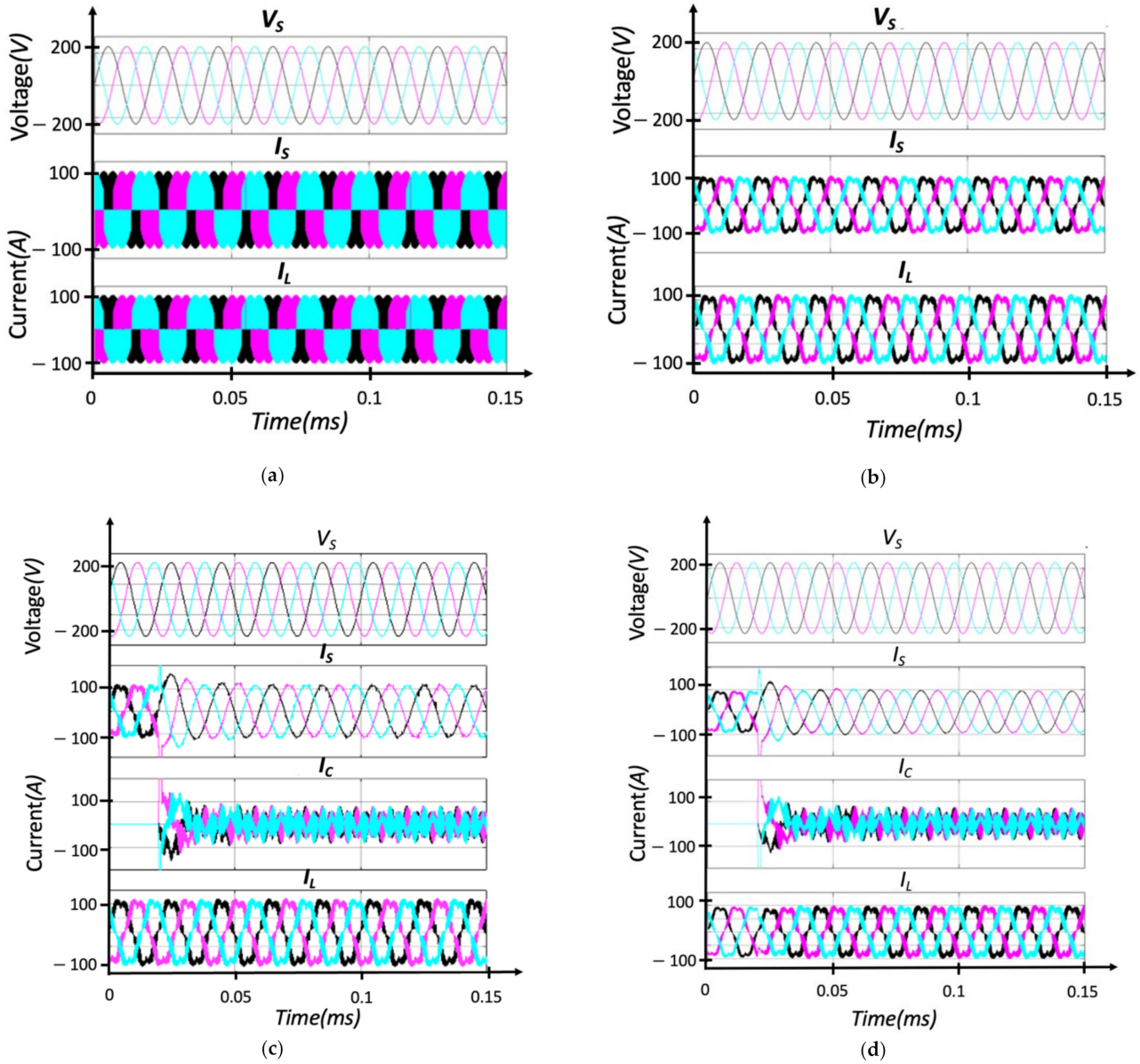

Figure 11. Setup with: (**a**) no filter; (**b**) passive R-L-C filter only; (**c**) HAPF with PI-controlled DC voltage; (**d**) HAPF with FIS-controlled DC voltage.

Figure 11c shows the shape of the three-phase supply voltage (*Vs*) and current (*Is*) as well as the compensating and load currents (I_C and I_L) of the setup with the PI-controlled SAPF. It could be observed that the supply voltage remained sinusoidal throughout the simulation time. In addition, after 20 ms of simulation time the supply current became sinusoidal and the load current remained distorted. The compensating current was highly distorted and 180° out of phase with the load current, which is most expected. FFT analysis of the supply current from Figure 12c indicated a 1.25% THD of the fundamental 50 Hz supply frequency. The higher ripple frequencies from the matrix converter were also recorded at the switching frequency with a reduced magnitude of the dominant harmonic, h155, as 0.15% of the fundamental. This shows a drastic improvement of the harmonic content in the supply current.

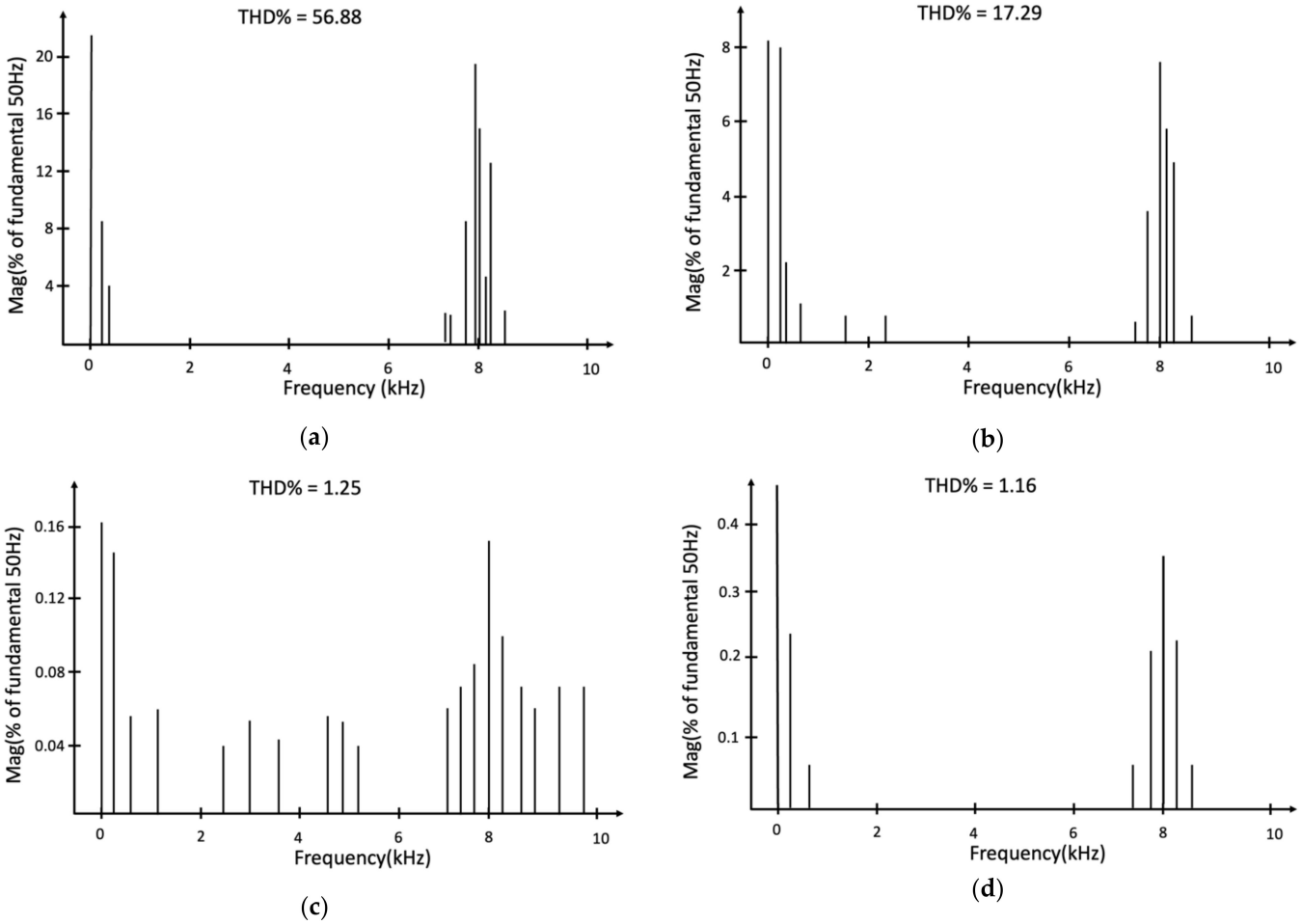

Figure 12. THD of the supply current: (**a**) without any filter action; (**b**) passive R-L-C filter only; (**c**) HAPF with PI-controlled DC capacitor voltage; (**d**) HAPF with FIS-controlled DC capacitor voltage.

Figure 11d shows the three-phase supply voltage (Vs) and its current (Is) shape, that of the compensating current (I_C), as well as the load current (I_L) of the setup with the FIS-controlled SAPF. While the supply voltage remained sinusoidal, the supply current became sinusoidal and in phase with the voltage after 20 ms of simulation time within half a cycle of settling time. FFT analysis of the supply current indicated a THD magnitude of 1.16% of the fundamental, and that of the dominant h155 from the MC as 0.37%, as shown in Figure 12d. Table 4 shows the comparison of harmonic contents before and after simulation under steady state operation for all scenarios.

Table 4. Comparison of results.

Simulation	THD% before Compensation	THD% after Compensation	THD% of Dominant 155th Harmonic before	THD% of Dominant 155th Harmonic after
R-L-C filter only	56.88	17.29	19.56	7.64
PI-controlled HAPF	56.88	1.25	19.56	0.15
FIS-controlled HAPF	56.88	1.16	19.56	0.37

6. Conclusions

High-frequency harmonics present in supply lines cause heating of transformers and motors, and interference with protective relays, metering devices and telecommunications equipment. The worst-case scenario is interference with hospital and laboratory setups

and measuring equipment. As applications of high-frequency transmission are increasing worldwide, and with the challenge of using the power lines as communication lines, there is a need to protect sensitive loads and equipment that are not equipped to handle high frequencies, particularly harmonic frequencies. The proposed fuzzy-controlled HAPF limits the high-frequency harmonics to the input side of the MC, thereby reducing the overall harmonic content of the supply current. The results obtained show a massive improvement in the harmonic content of the supply current in conformity with the recommended EMI and IEEE Std. 519-2014 requirements.

The proposed HAPF obtained less than half a cycle of response after active filter activation. The backbone of the HAPF is the appropriate control strategy for the generation of the compensational currents. This research employed the hysteresis control strategy which introduces limitations to the control of the switching frequency of the SAPF section of the HAPF. The solution would be to employ PWM-controlled SAPF, which will further introduce complexities to the design. This research is part of an ongoing investigation into supraharmonic frequencies generated by the matrix converter and their compensation using active filters. There is the possibility of further reducing the harmonic content of the line current, as well as the rate of change of the input current, with minimal use of passive elements and future works are aimed at that. Model predictive controllers exhibit promising results in inverter applications and future works are aimed at replicating their use in the active part of the proposed HAPF.

Author Contributions: Conceptualization, F.B.E.; methodology, F.B.E. and A.K.; software, A.K.; validation, F.B.E. and A.K.; formal analysis, F.B.E.; investigation, F.B.E. and A.K.; resources, F.B.E. and A.K.; writing—original draft preparation, A.K.; writing—review and editing, F.B.E. and A.K.; visualization, F.B.E. All authors have read and agreed to the published version of the manuscript.

Funding: This research received no external funding.

Conflicts of Interest: The authors declare no conflict of interest.

Nomenclature

C_{DC}	DC link capacitance
C_f	Passive filter capacitance
FIS	Fuzzy inferencing control system
HAPF	Hybrid active power filter
I_{MC}	Matrix converter current at grid frequency
I_S	Supply current
I_C	Compensating current
I_L	Load current
L_f	Passive filter inductance
L_C / L_{inv}	Active filter coupling inductance
MC	Matrix converter
SAPF	Shunt active power filter
S_{MC}	Matrix converter total power
V_S	Supply Voltage
VSC	Voltage source converter
ω	Grid frequency in radian
ω_C	Conner frequency in radian

References

1. Mutharasan, A.; Niranjan, K.; Rameshkumar, T.; Ajitha, A. Analysis of Power quality improvement in Matrix Converter for WEC System. *Int. J. Appl. Eng. Res.* **2014**, *9*, 11365–11372.
2. Karaca, H.; Akkaya, R. A Novel Hybrid Compensation Method Reducing the Effects of Distorted Input Voltages in Matrix Converters. *Elektron. Ir Elektrotech.* **2019**, *25*, 15–21. [CrossRef]
3. Chiang, G.T.; Itoh, J. Voltage Transfer Ratio Improvement of an Indirect Matrix Converter by Single Pulse Modulation. In Proceedings of the 2010 IEEE Energy Conversion Congress and Exposition, Atlanta, GA, USA, 12–16 September 2010; p. 9. [CrossRef]

4. Dabour, S.M.; Rashad, E.M. Improvement of Voltage Transfer Ratio of Space Vector Modulated Three-Phase Matrix Converter. In Proceedings of the 15th International Middle East Power Systems Conference, Alexandria, Egypt, 23–25 December 2012; pp. 581–586.
5. Goel, S.; Tiwari, D.; Pandey, M.K.; Bajpai, S. Power Quality Conditioners for Matrix Converter Using Shunt and Series Active Filters. *Int. J. Electron. Electr. Eng.* **2013**, *6*, 119–130.
6. Li, D.; Wang, T.; Pan, W.; Ding, X.; Gong, J. A comprehensive review of improving power quality using active power filters. *Electr. Power Syst. Res.* **2021**, *199*, 107389. [CrossRef]
7. Paul, P.J. Shunt Active and Series Active Filters-Based Power Quality Conditioner for Matrix Converter. *Adv. Power Electron.* **2011**, *2011*, 930196. [CrossRef]
8. Karaman, O.A.; Erken, F.; Cebeci, M. Decreasing Harmonics via Three Phase Parallel Active Power Filter Using Online Adaptive Harmonic Injection Algorithm. *Teh. Vjesn.—Tech. Gaz.* **2018**, *25*, 157–164. [CrossRef]
9. Wakileh, G.J. Effects of Harmonic Distortion on Power Systems. In *Power Systems Harmonics*; Springer: Berlin/Heidelberg, Germany, 2001; pp. 81–104. [CrossRef]
10. Shah, A.; Vaghela, N. Shunt Active Power Filter for Power Quality Improvement in Distribution Systems. *Int. J. Eng. Dev. Res.* **2005**, *13*, 22–26.
11. Koduah, A.; Svinkunas, G. Switching Harmonic Ripple Attenuation in a Matrix Converter-Based DFIG Application. In Proceedings of the 2022 IEEE 7th International Energy Conference (ENERGYCON), Riga, Latvia, 9–12 May 2022; pp. 1–7. [CrossRef]
12. Yanchenko, S.; Meyer, J. Impact of Network Conditions on the Harmonic Performance of PV Inverters. In Proceedings of the 2018 Power Systems Computation Conference (PSCC), Dublin, Ireland, 11–15 June 2018; pp. 1–7. [CrossRef]
13. Klatt, M.; Stiegler, R.; Meyer, J.; Schegner, P. Generic frequency-domain model for the emission of PWM-based power converters in the frequency range from 2 to 150 kHz. *IET Gener. Transm. Distrib.* **2019**, *13*, 5478–5486. [CrossRef]
14. Meyer, J.; Haehle, S.; Schegner, P. Impact of higher frequency emission above 2kHz on electronic mass-market equipment. In Proceedings of the 22nd International Conference and Exhibition on Electricity Distribution (CIRED 2013), Institution of Engineering and Technology, Stockholm, Sweden, 10–13 June 2013; p. 0999. [CrossRef]
15. Choudhary, J.; Singh, D.K.; Verma, S.N.; Ahmad, K. Artificial Intelligence Based Control of a Shunt Active Power Filter. *Procedia Comput. Sci.* **2016**, *92*, 273–281. [CrossRef]
16. Kaufhold, E.; Meyer, J.; Schegner, P. Impact of harmonic distortion on the supraharmonic emission of pulsewidth modulated single-phase power electronic devices. *Renew. Energy Power Qual. J.* **2021**, *19*, 577–582. [CrossRef]
17. Bollen, M.H.J.; Ribeiro, P.F.; Anders Larsson, E.O.; Lundmark, C.M. Limits for Voltage Distortion in the Frequency Range 2 to 9 kHz. *IEEE Trans. Power Deliv.* **2008**, *23*, 1481–1487. [CrossRef]
18. *IEEE Std 519-1992*; IEEE Recommended Practices and Requirements for Harmonic Control in Electric Power Systems. Institute of Electrical and Electronic Engineers: New York, NY, USA, 1992.
19. Casadei, D.; Serra, G.; Tani, A.; Zarri, L. Stability analysis of electrical drives fed by matrix converters. In Proceedings of the IEEE International Symposium on Industrial Electronics ISIE-02, L'Ayuila, Italy, 8–11 July 2002; Volume 4, pp. 1108–1113. [CrossRef]
20. Petrauskas, G.; Svinkunas, G. Innovative Filter Topology for Power Grid Protection from Switching Ripple Harmonics Produced by Matrix Converter. *Iran. J. Sci. Technol. Trans. Electr. Eng.* **2018**, *43*, 495–505. [CrossRef]
21. Monteiro, J.; Silva, J.F.; Pinto, S.F.; Palma, J. Matrix Converter-Based Unified Power-Flow Controllers: Advanced Direct Power Control Method. *IEEE Trans. Power Deliv.* **2011**, *26*, 420–430. [CrossRef]
22. Monteiro, J.; Pinto, S.; Delgado Martin, A.; Silva, J. A New Real Time Lyapunov Based Controller for Power Quality Improvement in Unified Power Flow Controllers Using Direct Matrix Converters. *Energies* **2017**, *10*, 779. [CrossRef]
23. Siva, B.V.; Babu, B.M.; Srinivas, L.R.; Tulasiram, S.S. Design of Shunt Active Power Filter for Improvement of Power Quality with Artificial Intelligence Techniques. *Int. J. Adv. Res. Electr. Electron. Instrum. Eng.* **2014**, *3*, 11304–11314. [CrossRef]
24. Koduah, A.; Svinkunas, G.; Ampofo, D.O. Design of a Shunt Active Power Filter for Direct Matrix Converter Application. In Proceedings of the 2021 IEEE PES/IAS PowerAfrica, Nairobi, Kenya, 23–27 August 2021; pp. 1–5. [CrossRef]
25. Alali, M.A.E.; Chapuis, Y.-A.; Saadate, S.; Braun, F. Advanced common control method for shunt and series active compensators used in power quality improvement. *IEE Proc.—Electr. Power Appl.* **2004**, *151*, 658. [CrossRef]
26. Janabi, A.; Wang, B. Hybrid matrix converter based on instantaneous reactive power theory. In Proceedings of the IECON 2015—41st Annual Conference of the IEEE Industrial Electronics Society, Yokohama, Japan, 9–12 November 2015; pp. 003910–003915. [CrossRef]
27. Jain, S.K.; Agrawal, P.; Gupta, H.O. Fuzzy logic controlled shunt active power filter for power quality improvement. *IEE Proc.—Electr. Power Appl.* **2002**, *149*, 317–328. [CrossRef]
28. Akagi, H.; Watanabe, E.H.; Aredes, M. *Instantaneous Power Theory and Applications to Power Conditioning*, 2nd ed.; IEEE Press/Wiley: Hoboken, NJ, USA, 2017.
29. Watanabe, E.H.; Monteiro, L.F.C.; Aredes, M.; Akagi, H. Instantaneous p-q Power Theory for Control of Compensators in Micro-Grids. In Proceedings of the 2010 International School on Nonsinusoidal Currents and Compensation, Lagow, Poland, 15–18 June 2010; p. 11.
30. Bissey, S.; Jacques, S.; Le Bunetel, J.-C. The Fuzzy Logic Method to Efficiently Optimize Electricity Consumption in Individual Housing. *Energies* **2017**, *10*, 1701. [CrossRef]

31. Roy, R.B.; Cros, J.; Basher, E.; Taslim, S.M.B. Fuzzy logic based matrix converter controlled indution motor drive. In Proceedings of the 2017 IEEE Region 10 Humanitarian Technology Conference (R10-HTC), Dhaka, Bangladesh, 21–23 December 2017; pp. 489–493. [CrossRef]
32. Tsengenes, G.; Adamidis, G. Shunt active power filter control using fuzzy logic controllers. In Proceedings of the 2011 IEEE International Symposium on Industrial Electronics, Gdansk, Poland, 27–30 June 2011; pp. 365–371. [CrossRef]